Materials Chemistry and Physics 112 (2008) 984–990

Contents lists available at ScienceDirect

Materials Chemistry and Physics

journal homepage: www.elsevier.com/locate/matchemphys

Optical properties and extinction spectroscopy to characterize the synthesis of amine capped silver nanoparticles

María Virginia Roldán[a], Lucía B. Scaffardi[b,c], Oscar de Sanctis[a], Nora Pellegri[a,*]

[a] Laboratorio de Materiales Cerámicos, FCEIyA, IFIR, UNR, Rosario, Argentina
[b] CIOp (CONICET, CIC), c.c. 124, 1900 La Plata, Argentina
[c] Área Departamental de Ciencias Básicas, Facultad de Ingeniería, Universidad Nacional de La Plata, La Plata, Argentina

ARTICLE INFO

Article history:
Received 30 November 2007
Received in revised form 2 June 2008
Accepted 21 June 2008

Keywords:
Nanostructures
Chemical synthesis
Optical properties

ABSTRACT

The present work describes a method for preparation of Ag nanoparticles from chemical reduction of $AgNO_3$ in ethanol with ATS [*N*-[3-(trimethoxysilyl)propyl] diethylenetriamine] as surface modifier. We study the influence of different parameters such as concentration, time, temperature and reductor agents on the size and shape of the nanoparticles. We present the morphologic and structural characterization of samples by UV–vis extinction spectroscopy, Atomic Force Microscopy (AFM) and X-ray diffraction (XRD).

Particularly, using optical extinction spectroscopy, the present work shows the analysis of size evolution in the fabrication process of spherical silver nanoparticles. This evolution is studied as a function of the time elapsed between the beginning of the reaction and the extraction of the sample (temporal delayed synthesis), and as a function of the temperature during the chemical reaction. In both the cases, we propose the study of the plasmon width as a useful, simple and inexpensive method for analysis of the mean radius, specially, for values below 6 nm.

1. Introduction

Nanotechnology has been the subject of increased interest in the last years due to the optic, magnetic, electric and catalytic properties that present the metallic nanoparticles involved in the development of different nanodevices. Applications of these devices are diverse, and, in all cases, fabrication processes of nanoparticles are a matter of study [1]. In particular, there is a remarkable interest to produce silver nanoparticles dispersions at large scale. Several methods have been reported for metallic nanoparticles synthesis, including Ag ions chemical reduction in aqueous solutions with or without stabilizing agents [2–5], thermal decomposition in organic solvents [6], chemical and photo reduction in reverse micelles [7,8], "nanosphere lithography" (NSL) [5], radiation chemical reduction [9] and microwave assisted [10], with typical advantages and disadvantages in each case. Most of the procedures previously described, yield stable silver dispersions only at relatively low concentrations of metal. Hence, they are not suitable for large-scale manufacturing.

The present work describes a simple method to produce Ag nanoparticles in continuous media at low cost. Silver nanoparticles are obtained from $AgNO_3$ chemical reduction in ethanol, using an aminosilane as catalyst and colloidal suspension stabilizer. In previous works [11] this reaction was attained employing aminosilanes with different amine groups in alcoholic solution in order to achieve nanoparticles isolation and stable colloidal suspension to control size. These compounds were used in different $AgNO_3$:aminosilane ratios (w/w). Besides, aminosilanes work as surface modifiers that avoid particle agglomeration, and their action allows future manipulation of nanoparticles. The optimal behaviour was found for the ATS aminosilane with a $AgNO_3$:aminosilane ratio of 1:3–5.

Besides describing the chemical production technique, this work presents a method to determine the core mean radius of the produced nanoparticles using optical extinction spectroscopy. The spectra are interpreted in terms of Mie's Theory using a model for the optical properties of silver nanoparticles that takes into account a modification of the dielectric function due to size effect [12,13].

2. Experimental

This work presents a method for preparation Ag nanoparticles from chemical reduction with alcohols. In a typical synthesis procedure, a solution around 0.008 M of $AgNO_3$ in different solvents and separately a solution of *N*-[3-(trimethoxysilyl)propyl] diethylenetriamine, Aldrich Tech (hereafter ATS) in ethanol under N_2 atmosphere are prepared. Subsequently, both solutions are mixed in equal quantities and a reflux with N_2 atmosphere at different temperatures (30–60 °C) is performed under vigorous stirring. A yellow-like stable solution was obtained and the Ag nanoparticles covered with ATS in ethanolic solution were stored in amber flasks.

* Corresponding author.
E-mail addresses: vroldan@fceia.unr.edu.ar (M.V. Roldán), pellegri@fceia.unr.edu.ar (N. Pellegri).

0254-0584/$ – see front matter © 2008 Elsevier B.V. All rights reserved.
doi:10.1016/j.matchemphys.2008.06.057

There are two methods of preparation of the samples: one, where the silver nanoparticles are reduced in ethanol (method I), and other, where the particles are reduced in methanol–acetone and redispersed in ethanol (method II).

The evolution of the solutions (progress of reduction reaction and size behaviour of silver nanoparticles) was analyzed by UV–vis extinction spectroscopy as a function of elapsed time, temperature, concentration and solvent employed. The absorption bands corresponding with the surface plasmons and bands of intermediate complex were studied during the nanoparticles formation [14], such as the absorption by complexes of Ag^+ and the Ag^{2+} intermediate reduced species or by small clusters of Ag^0 atoms. A spectrophotometer JASCO Model V-530 was employed to make UV–vis extinction spectra. These results are interpreted by a theoretical model based on size effects that modify optical properties of silver nanoparticles, especially for radii below 11 nm.

The morphologic characteristics of the nanoparticles obtained were investigated with AFM images. Samples were prepared by dropping a dispersion of the particles on a pristine HOPG substrate. The solvent evaporates naturally in air atmosphere and then the AFM measurements are taken. The AFM images were obtained in air at room temperature using a NanoTec electronica equipment with tapping mode configuration. A SiN tip supported by a silicon cantilever (0.76 N m^{-1} spring constant and 71 kHz resonance frequency) was used. Also, to compare and complete the results obtained from AFM analysis, Transmition Electron Microscopy (TEM) studies were made over samples prepared similarly to those for AFM, but over a TEM grid.

The crystalline structure of the nanoparticles was analyzed by X-ray diffraction technique with a Philips X-Pert Pro diffractometer using Cu Kα radiation (1.5405 Å) and a graphite monochromator (the step size being of $2\theta = 0.02^\circ$ and a 10 s time per step). The samples were prepared by depositing several drops of Ag nanoparticles suspension over a Si wafer and waiting for solvent evaporation. The difractometer was used with a grazing incidence configuration (GIXRD) using an angle of 0.5° or 1°.

3. Extinction spectra interpretation

The optical properties of materials are described by the complex dielectric function, $\varepsilon = \varepsilon' + i\varepsilon''$ which, in turn, can be written as two additives terms:

$$\varepsilon_{\text{bulk}}(\omega) = \varepsilon_{\text{bound-electron}}(\omega) + \varepsilon_{\text{free-electron}}(\omega) \quad (1)$$

where

$$\varepsilon_{\text{free-electron}}(\omega) = 1 - \frac{\omega_p^2}{\omega^2 + i\gamma_{\text{bulk}}\omega} \quad (2)$$

is the complex dielectric function for free electrons, ω_p is the bulk plasma frequency and γ_{bulk} is the damping constant in the Drude model. Values for $\omega_p = 1.38 \times 10^{16}\ s^{-1}$ and $\gamma_{\text{bulk}} = 2.7 \times 10^{13}\ s^{-1}$ were taken from reference [15].

As was mentioned in previous works [12,13] concerning small particles ($r <$ mean free path of conduction electrons in the bulk metal), the damping is strongly affected by size because the mean free path of the conduction electrons is dominated by collisions with the particle boundary, so it can be written as:

$$\gamma(r) = \gamma_{\text{bulk}} + C\frac{v_F}{r} \quad (3)$$

where v_F is the electron velocity at the Fermi surface, and r is the radius of the particle. The value $v_F = 14.1 \times 10^{14}\ \text{nm}\,s^{-1}$ was used [16]. C is a constant that includes details of the scattering processes. Its value can be determined from AFM measurement results as will be explained later. The C value ranges between 0.75 (for diffuse scattering) and 1 (for isotropic electron scattering). Thus, taking into account the dependence described by Eq. (3), the real and the imaginary part of the free electron contribution to the dielectric function for a particle of radius r can be written as:

$$\varepsilon'_{\text{size,free-electron}}(\omega, r) = 1 - \frac{\omega_p^2}{\omega^2 + \gamma^2(r)} \quad (4)$$

$$\varepsilon''_{\text{size,free-electron}}(\omega, r) = \frac{\gamma(r)\omega_p^2}{(\omega^2 + \gamma^2(r))\omega} \quad (5)$$

The size dependent dielectric function introduced in Eqs. (4) and (5) produces varied optical effects in the optical extinction spectra and consequently, in the plasmon width (FWHM), that allows to characterize the core radius of the nanoparticles.

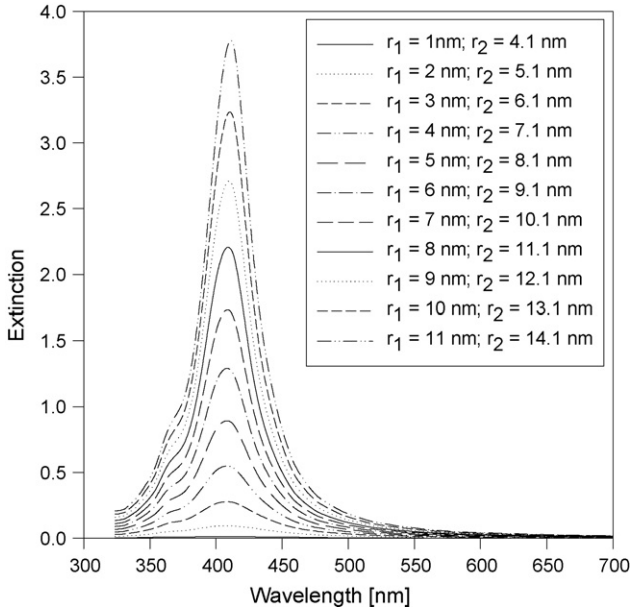

Fig. 1. Theoretical extinction spectra for silver nanoparticles capped with ATS stabilization agent immersed in ethanol, for radius lower than 11 nm, considering $C = 0.8$.

To calculate optical extinction spectra as a function of core radius for coated silver nanoparticles, we have considered $r_1 = r_{\text{core}}$ and $r_2 = r_{(\text{core+coating})}$ to distinguish the silver central core and the cladding with ATS stabilization agent. We have considered ethanol for the surrounding media.

Fig. 1 shows theoretical extinction curves obtained by Mie's Theory for $r_1 < 11$ nm and for a fixed coating thickness. The size dependent n and k values were calculated for Eqs. (4) and (5) considering $C = 0.8$ in Eq. (3) (see below). It can be seen that theoretically calculated plasmon peak position appears at 413 nm for a shell of 3.1 nm, and it can also be seen that it is weakly dependent on the core radius in this range. Since calculated extinction spectra for uncoated Ag Nps peak at 400 nm, it was necessary to consider that the ATS shell thickness is responsible for the red shift of the plasmon peak from 400 to 413 nm.

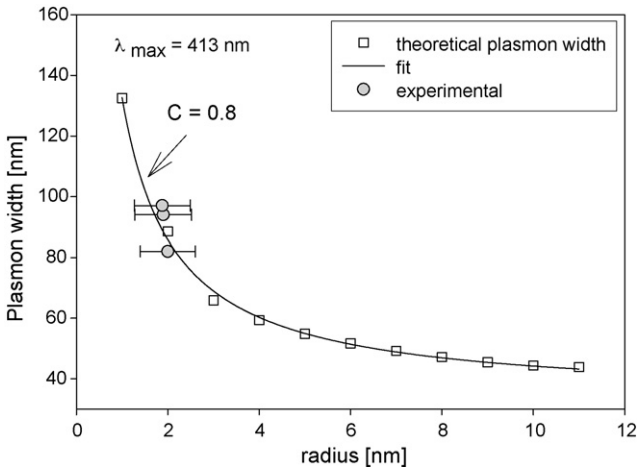

Fig. 2. Plasmon width FWHM (nm) as a function of radius of silver core nanoparticles. Squares are theoretical calculations considering $C = 0.8$ and grey circles are experimental values of plasmon width obtained by spectral extinction vs AFM measured radius. Errors bars correspond to AFM.

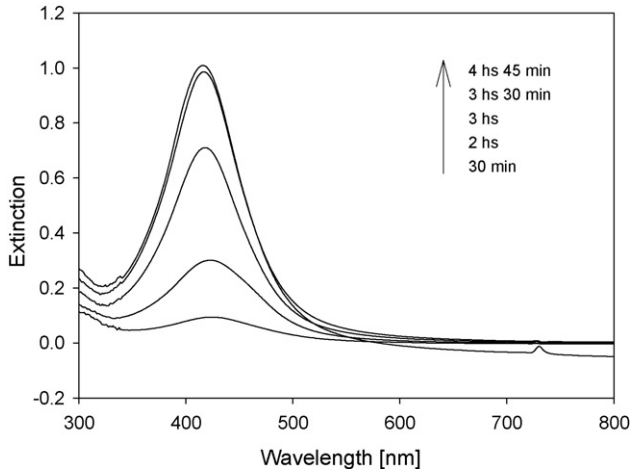

Fig. 3. Optical extinction spectra of silver capped nanoparticles for increasing sample extraction times starting from the beginning of the reaction.

Theoretical calculations show that the maximum shifts to larger wavelengths as the thickness increases. This resonance maximum tends to a stationary value for a thickness larger than 200% of core radius. For the case of 1 nm radius core silver particle, the considered thickness behaves almost equivalently to the surrounding medium.

It can be observed that the FWHM of the plasmon resonance calculated from spectral extinction, changes noticeably with the radius. This fact turns out to be useful to determine size of nanoparticles. The different C values generate a family of curves as a function of radius. In this sense, it is necessary to determine previously the C value using another experimental technique, as for example, microscopy. Fig. 2 shows the calculated FWHM as a function of core radius for $C = 0.8$. The white squares represent theoretical results. The grey circles represent three experimental values of plasmon width obtained from spectral extinction for different radii measured by AFM, since the described method only allows the fabrication of small Ag nanoparticles, typically less than 3 nm. Solid line shows the best fit of theoretical points. Notice that the three experimental circles lay in the steepest part of the graph and are fitted by the same curve.

It can be observed that while the plasmon width is approximately 140 nm for a spherical nanoparticle of 1 nm silver core radius, the value of the plasmon width decreases approximately to 47 nm for an 11 nm silver core radius. This dependence may be used as a calibration curve to characterize nanoparticles size.

In this sense, the analysis of plasmon width corresponding to experimental optical extinction and its comparison with theoretical curve shown in Fig. 2 can be used to determine radius of capped silver nanoparticles for values lower than 11 nm, and more specifically, for radius lower than 6 nm.

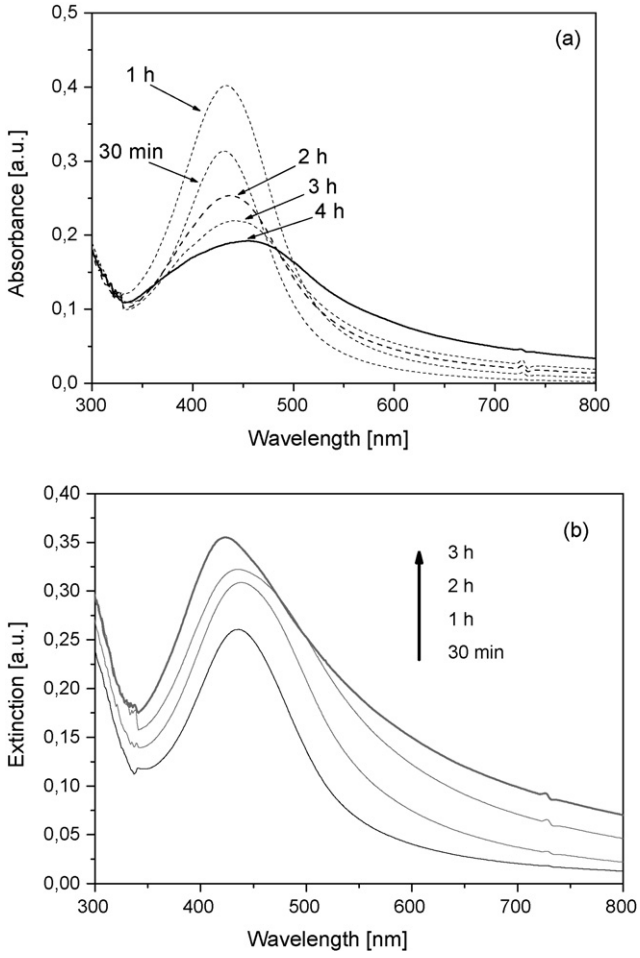

Fig. 5. Evolution of the UV–vis extinction spectra as a function of the elapsed time of the reaction: (a) for a diluted reaction medium ($AgNO_3$ = 2.5 mM, ATS = 8 mM) and (b) for a concentrated medium($AgNO_3$ = 8 mM, ATS = 26 mM).

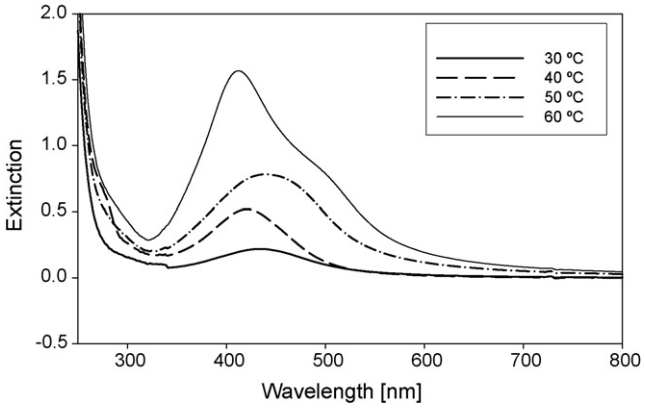

Fig. 4. Experimental UV–vis extinction spectra of ATS capped silver nanoparticles at different temperatures.

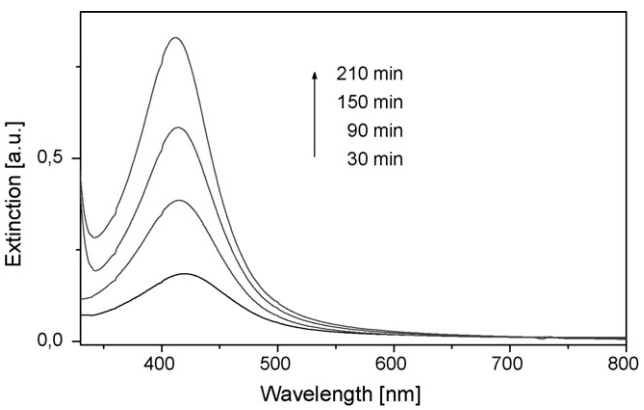

Fig. 6. UV–vis extinction spectra for different elapsed times, corresponding to method II.

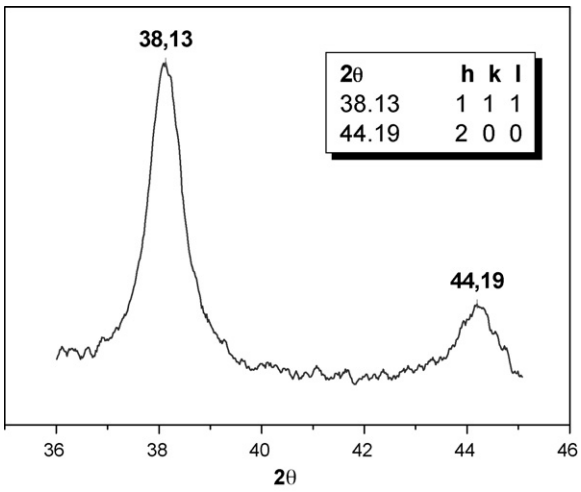

Fig. 7. X-ray difractogram corresponding to a sample prepared by method I.

4. Results

Using a simple technique of reduction in alcohol, yellow-like colloidal dispersions were obtained. The color is a consequence of the presence of fewnanometers radius Ag nanospheres, as will be shown later by microscopy images and theoretical calculations.

The evolution of nanoparticles formation was studied by UV–vis extinction spectroscopy. It is well known that for monodispersed spherical nanoparticles, only one plasmon band is obtained and the increase of its intensity is an indication of the reaction advance degree (Ag^+ to Ag^0 reduction) with the subsequent increment in the number of particles production.

We study the influence of different parameters such as reaction time, temperature, concentration and reductor agents in the fabrication process. On the other hand, we present results of size distribution by microscopy analysis, by X-ray diffraction (XRD) and finally, using optical extinction spectroscopy we determine the size distribution of nanoparticles for different times and temperatures.

To study the influence of the reaction time we follow the UV–vis extinction spectra of the reaction medium at different extraction times. Fig. 3 shows extinction spectra taken at several extraction times. It can be observed that nanoparticle formation begins at 30 min after reaction, suggested by the presence of a weak spectrum maximum around 424 nm. Besides, different plasmon widths (FWHM) for different extraction times are observed. The reaction reaches stabilization around 4 h, when the extinction spectra remain invariant with a peak near 413–416 nm. Samples were obtained from $AgNO_3$ at 4×10^{-3} M concentration and ATS surface modifier at 0.0125 M concentration.

The study of the temperature dependence was made between 30 and 60 °C. For the lowest temperature the reaction is poorly efficient, as shown in Fig. 4, where the surface plasmon band has very low intensity. For the highest temperatures (50 and 60 °C) the size distribution grows as suggested by the widening of the absorption band and a subsequent second peak appears for the highest temperature. The spectrum for 60 °C could be assigned to a bimodal distribution or non spherical shapes like rods, triangles, etc. However, by AFM analyses (not shown here) we only detected spherical nanoparticles with presence of large agglomerates together with small particles for the ones at 60 °C. On the other hand, there are no clues or signs that the ATS could act as a non-spherical shape promoter as other surface modifiers do. From the last results, the 40 °C production temperature was selected due to a good efficiency in reasonable time, obtaining a good nanoparticle size distribution as we will show later. In all cases the initial concentration of $AgNO_3$ in ethanol and the concentration of ATS remained constant. All samples were extracted 4 h after the beginning of the reaction.

In order to study the mixing concentration effect, a diluted and a concentrated media were analyzed maintaining the reactive ratio. By UV–vis extinction spectroscopy, a peak at 433 nm (nanoparticles presence, see Fig. 5a) is observed in a more diluted reaction medium than the concentration used for the experiment showed in Fig. 3. The absorption band grows quickly during the first reaction hour, but with the progress of the reaction it decreases in intensity. This behaviour indicates instability in particles production. When the synthesis was developed in a more concentrated medium than the conditions of Fig. 3 (Fig. 5b), stable nanoparticles suspension were obtained (the plasmon band grows continuously during the reaction time), but the efficiency was poor, on comparing the peaks intensity of Figs. 5b and 3 for the same time.

The best results were obtained for $AgNO_3$ 0.004 M and ATS 0.0125 M concentrations. The nanoparticles systems obtained under these conditions were stable, which ensure proper storage

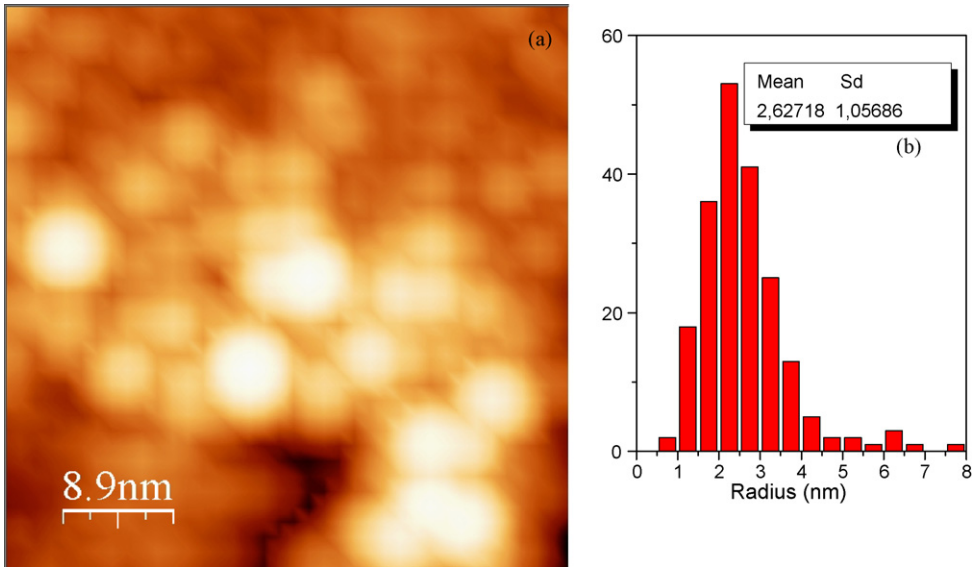

Fig. 8. (a) AFM image corresponding to silver nanoparticles reduced in ethanol, method I and (b) histogram of image (a).

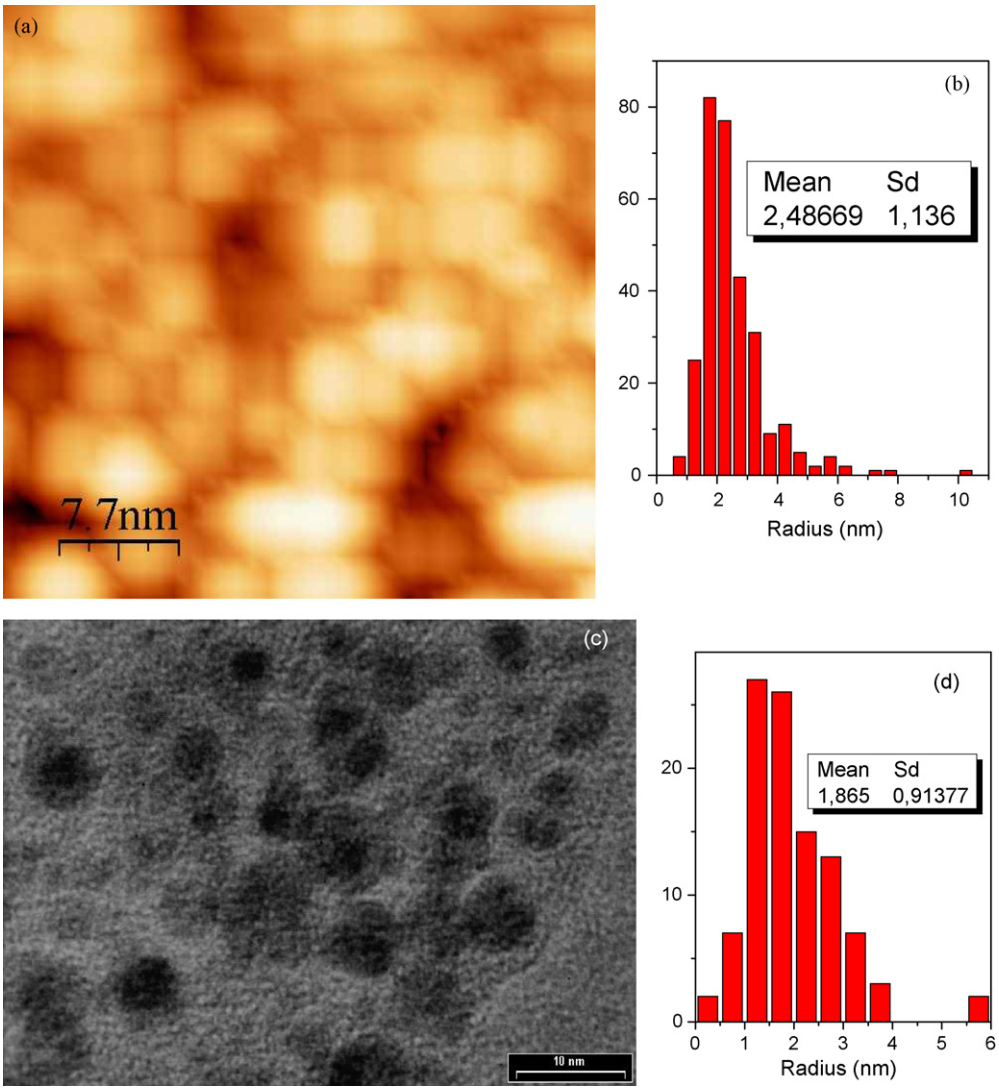

Fig. 9. (a) AFM images for the method II, (b) histogram of image (a), (c) TEM image for the method II and (d) histogram of image (c).

and handling for future uses in more complex systems like doped inorganic matrices [17–19].

In this preparation method, ethanol acts as solvent and as a mild reducing agent simultaneously. On the other hand, the ATS acts mainly as surface modifier, avoiding agglomeration of reduced Ag^0, coordinating with Ag^+ ions adsorbed over the nanoparticles surfaces through the amine groups. Previous works showed that this interaction between ATS and nanoparticles acts as helping the reaction in the reduction direction of the Ag nanoparticles [11]. Moreover, other authors have used amines as reducing agents in the formation of gold nanoparticles [20]. In this case the use of a compatible surface modifier with the sol–gel matrices through the terminal silane groups of the ATS, keep all the nanoparticles unaltered for further incorporation in optical coatings [17]. To study the effect of the solvent over the reaction time and the stability of the obtained product, a mix of acetone–methanol was employed. As mentioned earlier, nanoparticles produced with ethanol correspond to Method I and those produced with acetone–methanol, to Method II. From the UV–vis extinction spectra analysis (Fig. 6), spherical nanoparticles similar to those in ethanol were obtained, but with a narrow absorption band. This could be due to a decrease in the number of active sites for the reduction that is favourable to more soft and controllable reaction. The time to complete the reaction was approximately 4 h, similar to the one in ethanol.

In order to study the crystallinity Fig. 7 shows the XRD spectra of nanoparticles system prepared on Si wafer as a substrate. An FCC structure is revealed for the Ag^0 particles with 2θ values of 38.13

Table 1
Experimental plasmon width FWHM of extinction spectra corresponding to the elapsed times of Fig. 3

Elapsed time	FWHM (nm)
30 min	142
2 h	101
3 h	85
3 h:30 min	83
4 h:45 min	83

Table 2
Experimental plasmon width FWHM of extinction spectra corresponding to different temperatures of Fig. 4

Temperature (°C)	FWHM (nm)
30	123
40	101
50	142

Table 3
Core mean radius corresponding to different elapsed time from the analysis of the experimental plasmon width

Elapsed time	Calculated core mean radius (nm)
30 min	1.0 ± 0.6
2 h	1.5 ± 0.6
3 h	2.0 ± 0.6
3 h:30 min	2.1 ± 0.6
4 h:45 min	2.1 ± 0.6

and 44.19°, corresponding to the (1 1 1) and (2 0 0) crystalline planes respectively. The broad nature of the XRD peaks could be attributed to the nano-size of the particles [21]. The use of Scherrer analysis [22] of X-ray diffraction to calculate the nanoparticles size gives a mean radius of 5.2 ± 1.2 nm. Later, we will discuss this result.

AFM images were taken in order to study the particles size distribution. Fig. 8(a) shows the AFM image corresponding to a sample prepared using method I described above. Fig. 8(b) corresponds to the histogram showing a value of 2.6 nm ± 1.0 nm for the mean radius. This value is overestimated due to the fact that the AFM image includes the ATS capping layer, and the image was made taking into account the correction for the tip convolution and filters using WS&S software. For method II, similar AFM and TEM images with corresponding histograms were obtained. Fig. 9(a and b) shows an AFM image with a 2.5 nm ± 1.1 nm mean radius histogram, while Fig. 9(c and d) corresponds to TEM image with 1.9 ± 0.9 nm mean radius histogram. These results were used to determine the C value ($C = 0.8$) used for theoretical optical extinction calculations, a value close to that expected from the literature [15].

Finally, if we compare the mean size of the Ag nanoparticles estimated by microscopic techniques and XRD, it seems that the Scherrer calculus overestimated the radius. This fact is due to the fact that the sample is polydisperse and the XRD is particularly sensitive to the largest particles or crystallites [23]. Then, it is reasonable that the XRD results would be near the range end top of the AFM size analysis (see Fig. 8b).

5. Mean radius by optical extinction spectroscopy

Plasmon widths obtained from experimental extinction spectra corresponding to different samples of capped silver nanoparticles can be fitted by using plasmon widths of theoretical optical extinction curves, which depend on the radius. Theoretical extinction spectra calculated from Mie's theory are obtained for discrete wavelength values for which the silver refractive index is known from the literature [24]. The extinction spectra were calculated for different core mean radius (r_{core}), with 3.1 nm for the ATS cladding thickness and a C value appropriately determined. Theoretical plasmon widths taken from the calculated extinction spectra were compared with experimental plasmon widths obtained from extinction spectra of different samples which were analyzed using AFM and TEM microscopy. The samples prepared by the two methods mentioned above were used to determine the value of C.

As can be observed in Fig. 2, the grey circles represent the experimental plasmon width (FWHM in nm) obtained by spectral extinction as a function of the mean radius observed by AFM and TEM microscopy. The AFM images show nanoparticle morphology. Although in AFM images, particles seem to be very close to each other, they keep their morphology and individuality, and this is clearly observed in the spherical geometry of the particles. This characteristic is typical of different areas in the sample, with high or low population density of nanoparticles.

From Fig. 3 that shows experimental optical extinction spectra for different sample extraction times, different values of the plasmon width for each case that are summarized in Table 1 can be observed.

Fig. 4 shows experimental optical extinction curves of ATS capped silver nanoparticles at different fabrication temperatures. Analysis of the plasmon width is given in Table 2.

As was mentioned above, the analysis of the experimental plasmon width summarized in Tables 1 and 2, and its comparison with theoretical calculation allows us to determine the core radius of capped silver nanoparticles, in particular, below 6 nm. By using the curve that fits the theoretical plasmon width calculated for different core radius showed in Fig. 2, and using the measured experimental plasmon width from Tables 1 and 2, it is possible to calculate the radii of the particles synthesized by the above mentioned methods. We can summarize the results as follows in Tables 3 and 4.

The results shown in the 2nd column of Tables 3 and 4 are in agreement with the expected results from the method used for preparation samples, growing size with time and temperature. Nevertheless, the small radius for 50 °C obtained from these calculations are not in agreement with the experience. We believe that the use of this model is not applicable when the size distribution is very wide or bimodal. The described fabrication methods yield small radius particles (around 2 nm).

Finally we can conclude that the application of extinction spectroscopy for size characterization of synthesis and evolution of silver nanoparticles, using particularly the study of the plasmon width is possible. This method offers complementary information with respect to other mentioned techniques, especially on line monitoring capacity.

Table 4
Core mean radius corresponding to temperature evolution from the analysis of the experimental plasmon width

Temperature (°C)	Calculated core mean radius (nm)
30	1.1 ± 0.6
40	1.5 ± 0.6
50	<1 ± 0.6

6. Conclusions

Ag nanoparticles dispersions ranging between 2.1 and 1 nm average radius were obtained by chemical reduction of $AgNO_3$ in an aminosilane alcoholic solution. Colloidal solutions are stable for long periods and ATS aminosilane acts as surface modifier and catalytic reactor of Ag nanoparticles, inhibiting their growth and avoiding aggregation.

Optical extinction spectroscopy enabled size determination by analyzing the FWHM of the resonance plasmon peak as a function of radius. FWHM as a function of radius can be calculated from Mie's theory by proper modification of the Drude damping constant. The curve obtained in this way may be used to characterize silver nanoparticles size. This method constitutes an inexpensive, simple and very useful technique to size silver nanoparticles produced in different experimental conditions with a narrow size distribution. It was possible to follow the evolution of the fabrication process using this method.

Acknowledgments

The authors would like to thank Troiani, Horacio from Centro Atómico Bariloche (CNEA), Argentina for the TEM images. This work was partially performed with the aid of grants PICT 20466 and PICT 26090 from the Agencia Nacional de Promoción Científica y Tecnológica (ANPCyT), PIP 5302 and PIP 5997 from CONICET and

grants 11X/456 and 11I/104 from Universidad Nacional de La Plata, Argentina.

References

[1] I. Capek, Adv. Colloid Interf. Sci. 110 (2004) 49.
[2] L.M. Liz Marzan, I. Lado-Tourino, Langmuir 12 (1996) 3585.
[3] D.G. Duff, G. Baiker, P.P. Edwards, Langmuir 9 (1993) 2301.
[4] D.N. Glavee, K.J. Klabunde, C.M. Sorensen, G.C. Hadjipanayis, Langmuir 9 (1993) 162.
[5] I. Sondi, D.V. Goia, E. Matijevi, J. Colloid Interf. Sci. 260 (2003) 75.
[6] K. Esumi, T. Tano, K. Torigoe, K. Meguro, Chem. Mater. 2 (1990) 564.
[7] H.W. Lu, S.H. Liu, X.L. Wang, X.F. Qian, J. Yin, Z.K. Zhu, Mat. Chem. Phys. 81 (2003) 104.
[8] R. Trbojevich, N. Pellegri, A. Frattini, O. de Sanctis, P.J. Morais, R. Almeida, J. Mater. Res. 17 (8) (2002) 1973.
[9] A. Henglein, Langmuir 17 (2001) 2329.
[10] H. Katsuki, S. Komarneni, J. Mater. Res. 18 (4) (2003) 747.
[11] A. Frattini, N. Pellegri, D. Nicastro, O. de Sanctis, Mat. Chem. Phys. 94 (2005) 148.
[12] L.B. Scaffardi, N. Pellegri, O. de Sanctis, J.O. Tocho, Nanotechnology 16 (2005) 158.
[13] L.B. Scaffardi, J.O. Tocho, Nanotechnology 17 (2006) 1309.
[14] K. Lance Kelly, E. Coronado, L. Lin Zhao, G.C. Schatz, J. Phys. Chem. B 107 (2003) 668.
[15] U. Kreibig, J. Phys. F: Met. Phys. 4 (1974) 999.
[16] C.G. Granqvist, O. Hunderi, Phys. Rev. B 16 (1977) 3513.
[17] M.V. Roldan, N. Pellegri, A. Frattini, O. de Sanctis, Ferroelectrics 338 (2006) 127.
[18] N. Pellegri, R. Trbojevich, O. de Sanctis, K. Kadono, J. Sol–Gel Sci. Technol. 8 (3) (1997) 1023.
[19] M.V. Roldán, A. Frattini, O. de Sanctis, H. Troiani, N. Pellegri, Appl. Surface Sci. 254 (2007) 281.
[20] J.D.S. Newman, G.J. Blanchard, Langmuir 22 (2006) 5882.
[21] R. He, X. Qian, J. Yin, Z. Zhu, J. Mater. Chem. 12 (2002) 3783.
[22] H.P. Klug, L.E. Alexander, X-ray Diffraction Procedures for Polycrystalline and Amorphous Materials, John Wiley, New York, 1974.
[23] S. Calvin, S.X. Luo, C. Caragianis-Broadbridge, J.K. McGuinness, E. Anderson, A. Lehman, K.H. Wee, S.A. Morrison, L.K. Kurihara, Appl. Phys. Let. 87 (2005) 233102.
[24] E.D. Palik, Handbook of Optical Constants of Solids, vol. 1, Academic Press, New York, 1998, p. 350.